J Mater Sci (2008) 43:6857–6865
DOI 10.1007/s10853-008-3000-8

Effect of thermo-mechanical treatments on the microstructure of micro-alloyed low-carbon steels

M. Cabibbo · A. Fabrizi · M. Merlin · G. L. Garagnani

Received: 23 January 2008 / Accepted: 10 September 2008 / Published online: 27 September 2008

Abstract Micro-alloyed steels are known to exhibit superior mechanical properties through controlled rolling and specific thermo-mechanical treatments. Steel strength directly comes from a controlled precipitation process of carbides, nitrides and carbo-nitrides formed during the thermo-mechanical treatment, which are responsible for the fine-grained ferritic structure. In the present study, four different micro-alloyed, low-carbon steels have been studied: one baseline steel containing a small fraction of Al and N, and the other three with different fractions of Nb and V. Two thermo-mechanical treatments, which differed in the $\gamma \rightarrow \alpha$ transformation temperature were evaluated. Micro-strengthening contributions of the carbo-nitrides were determined using the Ashby-Orowan approach on the basis of TEM characterization. It was found that for the all four steels the Ashby-Orowan approach was in quite good agreement with the bulk yield strength (σ_y), as determined by mechanical testing steel (accounting for $0.8\sigma_y$). The pinning force of the particles was also calculated and compared to the recrystallization driving force. The steel containing Nb + V exhibited the highest pinning force, but the low fraction of the alloying elements, made this contribution only a fraction of $\sim$1/3 with respect to the recrystallization driving force.

M. Cabibbo (✉) · A. Fabrizi
Dipartimento di Meccanica, Università Politecnica delle Marche, Via Brecce Bianche 6131, Ancona, Italy
e-mail: m.cabibbo@univpm.it

M. Merlin · G. L. Garagnani
Dipartimento di Ingegneria, Università di Ferrara, Via Saragat 1, 44100 Ferrara, Italy

Introduction

The primary goal of a modern thermo-mechanical treatment is to refine the grain structure in order to obtain a good combination of mechanical properties in the hot-rolled condition in low-alloy, low-carbon steels. This follows from the fact that grain refinement is recognized as the only way to simultaneously improve both the strength and toughness. High-strength low-alloy (HSLA) steels have been developed over the past 40 years with wide range of applications in the pipeline, construction, automobile and pressure-vessel industries [1–4].

Grain refinement is obtained by careful control of the rolling conditions and time, temperature and deformation during the whole production process [1–7]. Controlled rolling of HSLA steels improve the mechanical properties to levels comparable to those pertaining to more highly alloyed heat-treated steels [7]. It has been demonstrated [1–8] for a variety of steel compositions that ultra-fine ferrite can be produced using the so-called strain-induced transformation rolling process. However, another way to achieve ferrite grain refinement is through dynamic recrystallization of ferrite during warm-working [7, 8]. A fine microstructure can also be produced in steels subjected to heat treatment, which combines warm-rolling and inter-critical annealing (carried out in the temperature region between Ac1 and Ac3) [7, 8].

Carbon is known to be the most important chemical element for strengthening steel, but it has detrimental effects on many technological properties such as weldability and formability. Therefore, the application of carbon-strengthened steels is rather limited. For wider application of cost-effective high-strength steels, it is generally recommend to other strengthening alloying elements for carbon [1–8]. Small additions of Nb, V and Ti are

well-known to induce grain refinement [5, 9–24]. The austenite grain boundaries are major ferrite nucleation sites, and, therefore, fine-grained austenite yields fine-grained ferrite. For this purpose, HSLA steels are usually alloyed with small quantities of strong carbide-forming elements such as Nb, V and Ti. The effect of these micro-alloying elements is to retard the progress of recrystallization by being dissolved in the austenite (solute-drag effect) or by forming precipitates (precipitation pinning effect) such that a fine ferrite grain structure can be produced eventually upon transformation [1–8]. These additions lead to a refinement of the microstructure and the precipitation of carbides or carbo-nitrides. Early formation of ultrafine nano-metric precipitates play an important role in nucleation processes of second-phase precipitates [9, 10] and in determining the mechanical properties of materials. It has been suggested that these nano-metric early precipitation (1–10 nm size) generate a network of elastically soft and relatively diffuse obstacles for the movement of dislocations. As a result, an increase in strength is achieved while maintaining good toughness [10].

Niobium is one of the most frequently added micro-alloying elements because of its strong effect on the improving microstructure and mechanical properties of steels. The state of niobium (in solution or in precipitate), determined by the reheating temperatures, can affect the recrystallization, the grain growth and the $\gamma \rightarrow \alpha$ transformation of austenite [3, 11, 12]. For example, the recrystallization and grain growth of austenite is significantly suppressed by the precipitation of NbC prior to the $\gamma \rightarrow \alpha$ transformation [3, 12]. In addition, coarse NbC particles can be preferred sites for ferrite nucleation. In particular, the control of the austenite recovery and recrystallization is an important part of the grain refinement technique in the modern thermo-mechanical controlling process [13]. The addition of Nb to a steel is considered to have three primary effects [14–18]: (i) as an inhibitor of austenite grain coarsening during reheating, (ii) suppression of austenite recrystallization prior to the $\gamma \rightarrow \alpha$ transformation through the strain-induced precipitation of NbC and (iii) precipitation hardening from the NbC in the low temperature transformation step of the thermo-mechanical process. The strongest contribution to the strengthening is the refinement of the final microstructure (essentially ferrite grain size), which accounts for 80–90% of σ_y. A key role of the precipitates is to provide dispersion strengthening, which is often generated in micro-alloyed steels by NbC, VC or Nb(C,N) or V(C,N) particles, depending on whether *N* is added or not, with less than 20 nm in size [10, 20–24].

As a retardation mechanism of austenite recrystallization, it has been proposed that the movement of subgrain boundaries is inhibited either by strain-induced carbo-nitrides precipitated during deformation [20] or by grain boundary segregation of micro-alloying elements. Austenite recovery is the stage prior of recrystallization, and since the movement of vacancies and climb of dislocations occur at this stage, dragging of these defects either by solute atoms [3, 21] or by very fine strain-induced precipitates, may be the reason for the retardation.

Special attention has also to be paid to vanadium micro-alloying addition. This element is easily added to liquid steel and its solubility during reheating is very high. The strengthening effect is enhanced as nitrogen is also added in solution [18, 19]. Vanadium provides grain refinement of austenite by carbo-nitride V(C,N) precipitation and improves the strength of steel by V(C,N) precipitation in ferrite during cooling.

The final microstructure and mechanical properties thus strongly depend on the chemical composition, the controlled rolling parameters and the cooling conditions to which the steel is subjected [24]. High strength, good ductility and good weldability are developed in steel products during manufacturing processes and to this goal properly balanced quantities of micro-alloying additions and suitable thermo-mechanical processing schedules have to be carefully applied [25, 26].

This article presents a microstructure study on the effect of two different thermo-mechanical treatments in four micro-alloyed low-carbon steels. The key objective of this study was to determine and discuss the strengthening contribution of the detected AlN, Nb(C,N), V(C,N) and NbV(C,N) carbo-nitrides in the four investigated steels subjected to a specific thermo-mechanical cycle.

Experimental procedures

Four types of low-alloyed, low-carbon steels were produced in terms of different content of Nb and V through Arvedi steel process[1] and then subjected to a specific

[1] The Arvedi steel process, first developed by Mannesmann Demag and Arvedi, is an in-line strip production technology. It is mainly constituted by a curved ingot mould, a secondary cooling station characterized by liquid core reduction, three stands in-line high reduction mill, a transversal cutters for the plate production, an induction heater and an intermediate winding-up heater station. The first reduction in thickness takes place during solidification in the course of the secondary cooling, when the slab's core is still liquid. The strip solidifies with a very fine-grained homogeneous microstructure without prevailing orientation. As a consequence, an improvement in the internal quality of the slab is realized ensuring better mechanical characteristics. Liquid core reduction also avoids macro-segregations of S, P and C and gives a better surface quality through a more effective powder lubrication in the ingot mould. The advantage in proceeding directly from the continuous casting to the in-line high reduction mill lies in the low milling rate (up to 0.1 m/s) which can eventually be reached. This low rate leads to a very high

Table 1 Chemical composition of the studied four micro-alloyed steels

Steel	C	Nb	V	N	Mn	Si	P	S	Al	$T_{\gamma\rightarrow\alpha}$ (°C)
Plain	0.043	–	–	0.008	0.18	0.04	0.005	0.002	0.045	570
Plain	0.04	–	–	0.009	0.19	0.03	0.005	0.001	0.042	690
Nb	0.045	0.012	–	0.01	0.27	0.05	0.006	0.002	0.038	590
Nb	0.044	0.023	–	0.008	0.20	0.03	0.005	0.002	0.045	675
V	0.044	–	0.039	0.009	0.48	0.02	0.006	0.001	0.039	580
V	0.044	–	0.039	0.009	0.48	0.02	0.006	0.001	0.039	680
Nb-V	0.05	0.015	0.025	0.009	0.51	0.07	0.006	0.001	0.051	580
Nb-V	0.05	0.015	0.025	0.009	0.51	0.07	0.006	0.001	0.051	680

The two different $\gamma \rightarrow \alpha$ transformation temperatures for the two thermo-mechanical treatments are also reported

thermo-mechanical treatment. Table 1 reports the chemical composition and the temperatures of the $\gamma \rightarrow \alpha$ transformation final rolling stage of the thermo-mechanical treatment reported in Fig. 1.

Optical microscopy was carried out on specimens mechanically polished and then chemically etched with a solution of Nital–2%. TEM discs were prepared from samples mechanically thinned to 100 μm in thickness. The 100-μm-thick discs were polished with a Struers™ dimple grinder and subsequently thinned to electron transparency

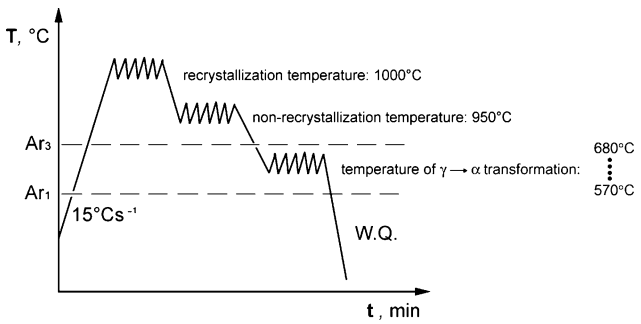

Fig. 1 Schematic representation of the thermo-mechanical treatments. All the four steels were subjected to two different $\gamma \rightarrow \alpha$ transformation temperatures ($T_{\gamma\rightarrow\alpha}$). Plain steel: $T_{\gamma\rightarrow\alpha} = 570$ °C (a) and 690 °C (b); Nb-bearing steel: $T_{\gamma\rightarrow\alpha} = 590$ °C (c) and 675 °C (d); V-bearing steel: $T_{\gamma\rightarrow\alpha} = 580$ °C (e) and 680 °C (f); Nb-V-bearing steel: $T_{\gamma\rightarrow\alpha} = 580$ °C (g) and 680 °C (h)

Footnote 1 continued
transversal flow of material, during the first passage of the work-mill with a reduction of up to 50%. Once the high reduction mill has been fed directly from the continuous caster, the intermediate slab goes into the induction heater and it is reheated to a suitable temperature to obtain the scheduled properties of the material. A main parameter of the induction heater is the temperature, since it can severely influence the formation of superficial defects, the possible precipitation or dissolution of new particles, the austenite grain size and its evolution during the subsequent high-temperature plastic deformation. These factors will therefore determine for the onset of rolling temperature.

using a Gatan Precision Ion Polishing System (PIPS™). TEM investigations were carried out using a Philips™ CM200 transmission electron microscope, operating at 200 kV, equipped with double tilt specimen holder and an energy dispersive X-ray spectrometer. Precipitate identification was performed using both convergent beam electron diffraction (CBED) and energy dispersive X-ray spectroscopy (EDS) spot analyses.

Carbo-nitrides precipitates approximately 50 nm in size were identified by CBED, and it was not possible to identify any precipitates finer than 20 nm in this study; for those, EDS spot analyses were carried out. Local thickness measurements of the electron-transparent foils were performed using the Kossel fringes method.

Statistical analysis was carried out with Image Pro Plus® V4,5 software on at least five TEM bright field images, for each experimental condition.

Yield, ultimate strengths and elongation were measured through room temperature tensile tests conducted using a MTS™ servo-hydraulic computer-assisted testing machine. Three specimens were tested for each experimental condition.

Experimental results

Figure 2 shows representative optical-microscopy images of the ferrite structure in the four different steels processed using the two different thermo-mechanical conditions.

Ferrite grains are fairly equiaxed with average sizes of 11 μm and 19 μm for the baseline steel after $\gamma \rightarrow \alpha$ deformation temperature of 570 °C and 690 °C, respectively; average sizes of 10 μm and 8 μm for the Nb-bearing steel after $\gamma \rightarrow \alpha$ deformation temperature of 590 °C and 675 °C, respectively; average sizes of 11 μm and 9 μm for the V-bearing steel after $\gamma \rightarrow \alpha$ deformation temperature of 580 °C and 680 °C, respectively; and an average size of 7 μm for the Nb-V steel after $\gamma \rightarrow \alpha$ deformation temperature of 580 °C and 680 °C. These values are in rather good agreement

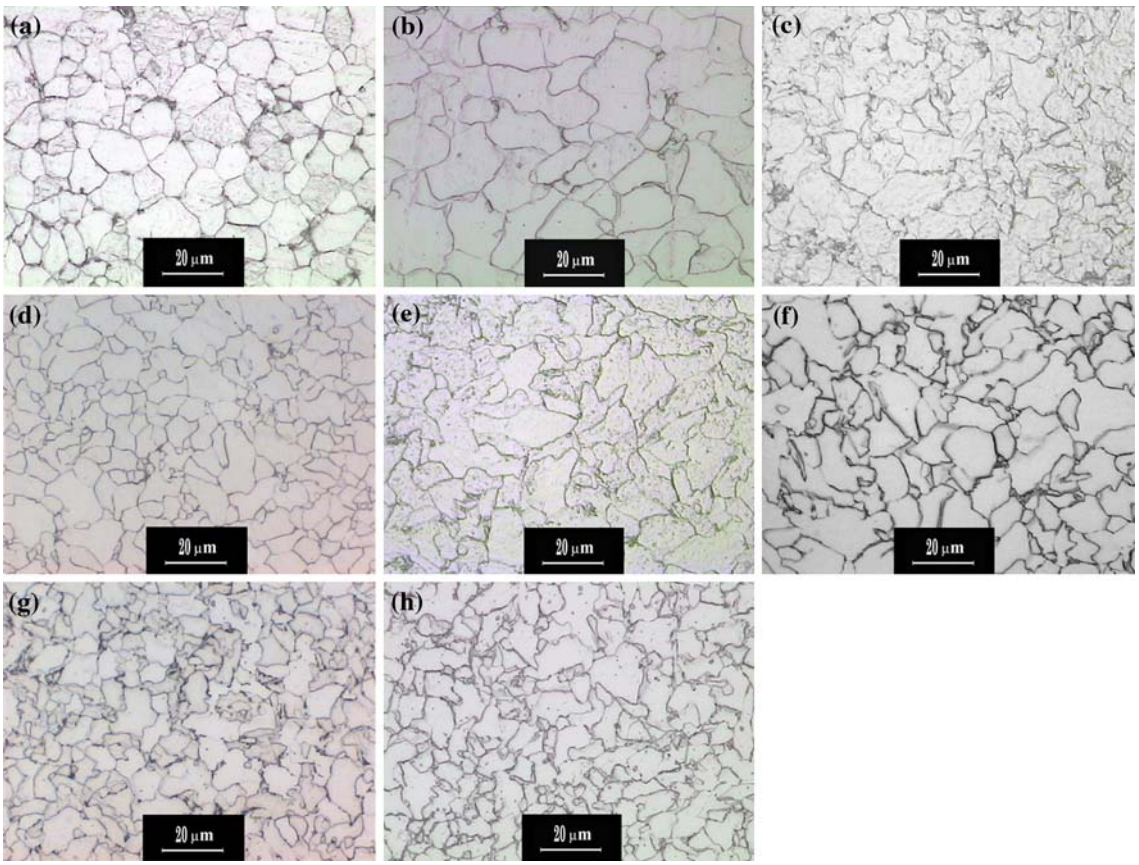

Fig. 2 Representative optical micrographs of the ferrite-grained structure at the different thermo-mechanical experimental conditions for the four steels. Plain steel at $T_{\gamma\to\alpha} = 570$ °C (**a**) and 690 °C (**b**); Nb-bearing steel at $T_{\gamma\to\alpha} = 590$ °C (**c**) and 675 °C (**d**); V-bearing steel at $T_{\gamma\to\alpha} = 580$ °C (**e**) and 680 °C (**f**); Nb-V-bearing steel at $T_{\gamma\to\alpha} = 580$ °C (**g**) and 680 °C (**h**)

to the data reported in [27] by Azevedo et al. for a C–Mn steel, obtained at the end of an industrial hot rolling process.

Ferrite recrystallization and particle precipitation are competing processes and progress of recrystallization can be halted by the drag exerted on the migrating grain boundaries by the presence of either solute Nb, V and Nb + V, depending on the alloying elements in the steel, or by Zener pinning exerted by the strain-induced precipitates preferentially nucleating on dislocation nodes as per the classical theory given by Dutta and Sellars [28]. The increase in the $\gamma \to \alpha$ temperature resulted in a slight coarsening of the ferrite grains in the baseline steel. In contrast, for the Nb-V-bearing steels, the grains were respectively reduced by increasing the $\gamma \to \alpha$ temperature from 590 °C to 675 °C and from 580 °C to 680 °C. In the Nb steel some deformation bands are also clearly visible. On the other hand, the ferrite grains of the Nb-V steel do not appear to be affected by the changing in $\gamma \to \alpha$ transformation temperature from 580 °C to 680 °C.

Figure 3 shows some representative TEM images of the precipitates formed after the thermo-mechanical treatments for the four different steels, corresponding to the eight different experimental conditions.

The plain carbon baseline steel was characterized by the presence of AlN precipitates. The rate of AlN precipitation in austenite, under isothermal conditions, reached a maximum at 1,000 °C (recrystallization temperature). The onset of the $\gamma \to \alpha$ transformation has a significant accelerating effect on the precipitation of AlN due to the faster diffusion and the lower solubility of Al in ferrite [19, 20, 23, 24, 26].

The vast majority of the particles in the Nb-bearing steel were identified as Nb(C,N) from selected area electron diffraction patterns (SAEDPs). Craven and co-workers [19] reported a stoichiometry of $NbC_{0.7}N_{0.3}$ for the Nb(C,N) carbo-nitrides, but in the present study no discerning of the exact ratio between C and N was possible by SAEDP or nano-probe EDS analysis. A minority fraction was detected as AlN. Together with the strain-induced Nb carbo-nitrides detected by TEM, a high number density of uniformly distributed ultrafine (2–10 nm) precipitates was also observed. These observations are also confirmed by the TEM work of Pereloma et al. [9].

In the V-bearing steel carbo-nitrides were identified as V(C,N). They were as abundant as the Nb(C,N) in the steel containing Nb. AlN particles were far less common than in the Nb-bearing steel probably due to a greater N affinity to V.

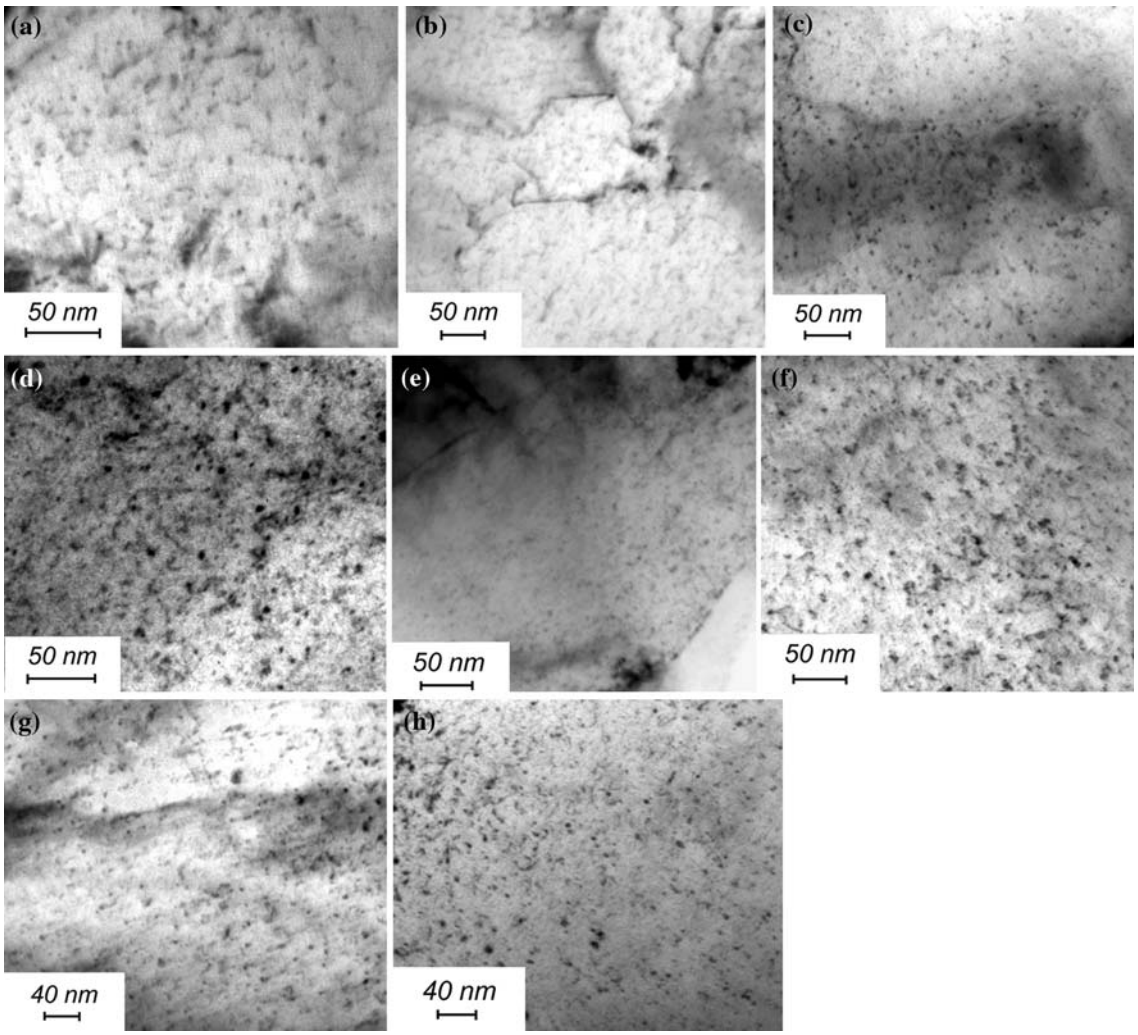

Fig. 3 Representative TEM images showing the AlN nitrides and the different carbo-nitrides in the four steels

The V-particle size ranged from 5 to 20 nm and few clusters were identified.

The microstructure of the Nb-V steel appears as rather fully decorated by fine nano-metric particles. Carbo-nitrides were identified as NbV(C,N). The interior of the ferrite grains were mostly populated by the nano-metric NbV(C,N) and some sporadic AlN particles. Their mean size was 14 nm and very few AlN needle-shaped particles were detected. The size range of the all carbo-nitrides was 5–20 nm and their identification was not possible simply on the basis of their morphology, but only through SAEDPs or nano-probe EDS analyses. As discussed by Houghton [29], the role of micro-alloying elements and the optimization of HSLA micro-alloyed steels design are based on the mutual solid solubility of carbides and nitrides. Complete miscibility is expected at high temperatures (>1,100 °C) for carbides and nitrides such as Nb(C,N), V(C,N) and NbV(C,N), while kinetic limitations are expected to prevent extensive precipitate homogenization during thermo-mechanical processing at lower temperatures (<1,100 °C) [29, 30]. In the present case, the scarce presence of C, Nb and V, made their mutual miscibility easier and complete precipitation (through the formation of carbo-nitrides particles and clusters) occurs already after the recrystallization temperature of 1,000 °C.

In order to correlate the yield strength, determined by the tensile tests [29], to the microstructural features, an analytical approach was followed utilizing TEM.

Typical yield strengths for the steels studied in this work are about 450 MPa [29]. This strength essentially comes from (i) the intrinsic resistance of the crystal structure (20 MPa), (ii) the refinement of the ferrite grain size (170 MPa), (iii) precipitation hardening (160 MPa) and from solid solution and dislocation hardening (100 MPa), this latter determined from literature data [29]. The value of 450 MPa is thus resulting assuming a simple summation without synergic effects. A description and evaluation of the yield strength of micro-alloyed steel in terms of the

microstructural features can be obtained by using the Ashby-Orowan approach (Eq. 1 and 2) [27, 28]:

$$\sigma_{\text{calc}} = \sigma_0 + \sum k_i c_i + k_y d_{\text{eq}}^{-1/2} + 3\sigma_{\text{Or}} \quad (1)$$

where

$$\sigma_{\text{Or}} = 3(0,81\text{Gb}/(2\pi(1-\nu)^{1/2})\ln(d_{\text{eq}}/b)/\lambda_{\text{eff}}) \quad (2)$$

σ_0 being the material' strength as a single crystal in the annealed condition, $\sum k_i c_i$ the contribution of the solid solution strengthening, k_i is the hardening coefficient for the i-th solute and c_i its concentration in %wt., $k_y d_{\text{eq}}^{-1/2}$ the hardening contribute due to the mean size of the grains, 3 is the Taylor factor, G the shear modulus (4×10^4 MNm^{-2}), b the Burgers vector (0.2 nm), ν the Poisson ratio (0.3), d_{eq} the mean equivalent diameter of the particles and λ_{eff} their mean lateral centre-to-centre spacing. In Table 2 are reported the statistical data (d_{eq}, V_v, λ_{eff}) for the AlN particles (plain steels), Nb(C,N), V(C,N) and NbV(C,N) for the three other micro-alloyed steels. No distinction between AlN and carbo-nitrides were made in the pinning strength calculation for three steels containing, Nb, V or Nb + V. Table 2 also reports the calculated σ_{calc} and the $\sigma_{\text{calc}}/\sigma_y$ ratio between it and the mechanically measured bulk yield strength.

By using Eqs. 1 and 2, the yield strength of the micro-alloyed steels were calculated in terms of the solute contents, the grain size contribution and the dispersion strengthening (mean particle diameter and volumetric fraction of particles), this latter being included in the centre-to-centre λ-spacing.

Figure 4 shows the yield strengths for the four steels and the eight different experimental conditions (in terms of alloying element and thermo-mechanical treatments) as determined mechanically and as calculated through the Eq. 1. The ultimate strength values are also reported. The values of the calculated microstructural strengthening were systematically lower by a factor of 10–20% with respect the mechanical yield strength. The most interesting aspect is that the discrepancy was limited to within the 20%. This

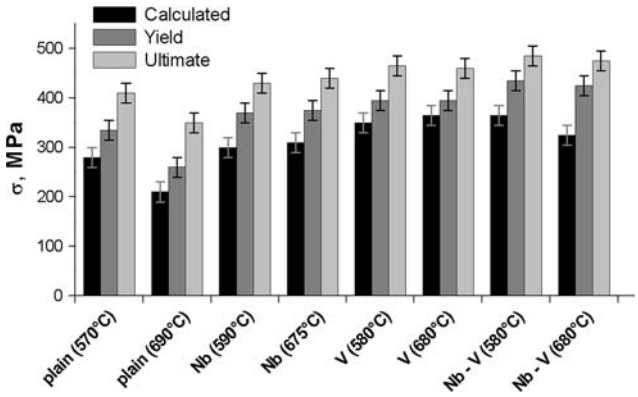

Fig. 4 Bar-plot of the calculated microstructure strength (σ_{calc}), through Eq. 1, against the yield and ultimate strengths as determined through mechanical tests

clearly shows the advantage of the calculcated micro-structural strengthening through the Ashby-Orowan approach.

Moreover, interrupted compression tests were conducted in order to estimate the driving force for recrystallization based on the differences in dislocation density ($\Delta\rho$) across the moving boundary [3], as follows:

$$F_R = \text{Gb}^2\Delta\rho/2 \quad (3)$$

where G is the shear modulus (4×10^4 MNm^{-2}) and b is the Burgers vector (0.2 nm). $\Delta\rho$ can be estimated through the following relationship [30]:

$$\Delta\sigma = 0.2\ \text{Gb}(\Delta\rho)^{1/2} \quad (4)$$

The pinning force exerted by the particles, against recrystallization, is expressed according to Zener and Gladman [3] as:

$$F_p = 2d_{\text{eq}}\gamma N_s \quad (5)$$

where d is the particle equivalent diameter, γ is the inter-facial energy per unit area of boundary (0.8 Jm^{-2}), and N_s is the number of particles (AlN, Nb(C,N), V(C·N) or NbV(C,N)) per unit area of boundary. The particle pinning

Table 2 Particle mean diameter, volume fraction, particle spacing and calculated microstructure strengthening (Eqs.1 and 2) for all the eight experimental conditions discussed in the article

The $\sigma_{\text{Or}}/\sigma_y$ ratio between the calculated Orowan strengthening (Eq. 1) and the measured yield strength is also reported

Steel	d_{eq} (nm)	λ_{eff} (nm)	V_v	σ_{calc} (MPa)	$\sigma_{\text{calc}}/\sigma_y$
Plain ($T_{\gamma\to\alpha}$ = 570 °C)	3.8	214	0.0051	280	0.81
Plain ($T_{\gamma\to\alpha}$ = 690 °C)	4.1	247	0.0047	210	0.78
Nb-bearing ($T_{\gamma\to\alpha}$ = 590 °C)	4.8	108	0.0091	302	0.83
Nb-bearing ($T_{\gamma\to\alpha}$ = 675 °C)	5.4	119	0.0098	308	0.82
V-bearing ($T_{\gamma\to\alpha}$ = 580 °C)	3.8	89	0.0059	349	0.88
V-bearing ($T_{\gamma\to\alpha}$ = 680 °C)	3.3	78	0.0054	362	0.93
Nb-V-bearing ($T_{\gamma\to\alpha}$ = 580 °C)	4.3	72	0.0103	363	0.82
Nb-V-bearing ($T_{\gamma\to\alpha}$ = 680 °C)	4.9	68	0.0105	331	0.79

Table 3 Particle pinning force and recrystallization driving force as calculated through Eqs. 3 and 5, respectively

The ration between the pinning force and the driving force is also shown

Steel	Particle pinning force (MNm^{-2})	Recrystallization driving force (MNm^{-2})	Ratio
Plain ($T_{\gamma\to\alpha} = 570$ °C)	0.41	4.35	0.094
Plain ($T_{\gamma\to\alpha} = 690$ °C)	0.36	4.06	0.089
Nb-bearing ($T_{\gamma\to\alpha} = 590$ °C)	0.58	2.15	0.270
Nb-bearing ($T_{\gamma\to\alpha} = 675$ °C)	0.56	2.31	0.242
V-bearing ($T_{\gamma\to\alpha} = 580$ °C)	0.47	3.45	0.136
V-bearing ($T_{\gamma\to\alpha} = 680$ °C)	0.48	3.19	0.151
Nb-V-bearing ($T_{\gamma\to\alpha} = 580$ °C)	0.74	2.05	0.360
Nb-V-bearing ($T_{\gamma\to\alpha} = 680$ °C)	0.65	2.21	0.293

force and the recrystallization driving force are reported in Table 3. The recrystallization driving force in plain steel is al least 50% higher than in the case of the other micro-alloyed steels and it is half compared to the Nb-V-steel. This is certainly due to the presence of the fine nano-metric carbo-nitrides and it implies that AlN are far from being as effective as the Nb(C,V) or V(C,N). The pinning force exerted by the particles are surprisingly close except for the NbV(C,N) carbo-nitrides that showed a noticeable stronger pinning force ($\sim$20%). The ratio between the pinning force and the recrystallization driving force clearly shows small contribution of these particles especially in the case of AlN (plain steel). The highest ratios of 0.360 and 0.293 are obtained for the NbV(C,N) particles at the $\gamma \to \alpha$ transformation temperature of 580 °C and 680 °C, respectively. This clearly reflects the scarce presence of alloying elements even for the Nb-V steel, as the particles pinning force only accounts for one-third of the recrystallization driving force (as determined by Kwon and DeArdo [3] for a Nb-V steel at $T_{\gamma\to\alpha} = 580$ °C).

Discussion

The most efficient practical method for implementation of grain refinement in HSLA steel is a controlled rolling process. It relies on processing the austenite in a temperature region of non-recrystallization, and/or ($\alpha + \gamma$) region, thus offering more nucleation sites for the transforming ferrite.

The chosen thermo-mechanical treatment for the four low-C, low-alloyed steels is based not only on deep-rooted industrial practices, but it is also supported by several published studies [1, 2, 31–36].

Two different treatments are proposed and discussed in [1]. The first schedule consists of reheating the steel to rolling temperature, rolling in the recrystallization region, rolling in the ($\gamma \to \alpha$) two-phase region and then final cooling. The second schedule differentiates from the first one on the final rolling which is done in the γ non-recrystallization region. Moreover, this second process schedule induced an impact toughness increment to the steel compared to toughness reached under the first schedule. The Bakkaloglu second process schedule is virtually identical to the one presented in this work (the only difference being in the recrystallization and $\gamma \to \alpha$ transformation temperatures). Similar results were obtained by Houghton [33] and Hong et al. [34].

In the present case, dynamic recrystallization occurs during the thermo-mechanical treatment at a relatively high temperature (1,000 °C), while at intermediate rolling temperatures ($\sim$950 °C) an incubation time for the formation of new equiaxed grains (static recrystallization) is needed [2, 3, 11, 13, 31, 37–44]. The strain which is needed for ferrite nucleating at the prior austenite grain boundary is different. In Nb-V-free steel (plain steel), the austenite grain boundary begins to be occupied by equiaxed ferrite grains, but in Nb-bearing steel ferrite grains mainly locate along the austenite grain boundaries or at a triple junction in the microstructure. This is also true for the thermo-mechanically treated Nb-V-steels. The driving force for recrystallization in all the eight experimental conditions (Table 3) clearly showed lower values for the micro-alloyed steels with respect to the baseline steel. In particular, the presence of Nb (Nb-bearing and Nb-V-bearing steels) is responsible for a greater driving force reduction. This because the thermo-mechanical treatments induce the precipitation of Nb carbo-nitrides, or Nb + V carbo-nitrides within the ferrite microstructure. These very fine precipitates are effective in preventing grain growth. The carbo-nitride particles were in the size range of 5–20 nm in all the experimental cases. In a few rare cases, ultrafine 2–5 nm in size Nb and V carbo-nitride precipitates were detected. The detected carbo-nitride particle sizes are in good agreement to the other authors findings. Burke et al. [37] used a combination of Atom probe field-ion microscopy and TEM to study Nb(C,N) precipitation in HSLA steel. They observed precipitates with diameters in the ranges 0.4–5 nm and 2–40 nm by APFIM and TEM, respectively. This work also showed that Nb(CN)

precipitates as fine as 2 nm could be detected by conventional TEM. The two techniques showed excellent agreement for precipitate size measurements. Kwon and De Ardo [3] reported mean particle sizes range from 4 to 10 nm, while, LeBon [17] reported a value of 3–4 nm, and Hansen [25] a value of 5 nm after holding of 1,000 s at 900 °C. However, Luton et al. [40] reported an average value of 25.9 nm (holding time of 20 s after a pre-strain of 0.25 at 0.01 s^{-1}) and Yamamoto et al. [44] (at a temperature of 1,000 °C) a mean size of 25 nm. On the other hand, a variety of particles were observed [31]: (i) relatively coarse of cuboidal and needle-like shape; (ii) spherical or elongated particles at grain or subgrain boundaries; and (iii) fine precipitates within ferrite grains. The EDS analyses in [31] of such particles, performed out of carbon extraction replica, showed that these also contain some Fe in addition to Nb and Ti.

Hong and co-workers [11] stated that Nb precipitates in austenite accelerated the ferrite transformation as they could act as potential nucleation sites, and they were also responsible for decreasing the carbon content in the austenite, thus promoting the ferrite transformation. The suppression of grain boundary migration due to micro-alloying is caused by either the solute dragging effect caused by segregation of alloying elements to the boundaries, or the pinning effect caused by carbo-nitride precipitates [45–58]. Kwon and De Ardo [3] reported that the retardation in the process of recrystallization is attributed to the early formation (within few seconds) of Nb(C,N) particles before the start of recrystallization.

The localized distribution of Nb(C,N) particles, detected by TEM in the present study, appears to be a characteristic of Nb(C,N) precipitation in deformed austenite, i.e. the final distribution reflects the homogeneous nature of the precipitate nucleation process. The precipitation of Nb(C,N) at the prior austenite grain boundaries is in agreement with the observations of Hansen et al. [25] and Crocks et al. [52]. However, in the present study, the localized particles were more frequently observed within the grains, delineating what may be the location of subgrain boundaries. It then appears that the precipitation of Nb(C,N) is likely to occur at both deformation bands and austenite subgrain boundaries. Thus, the more frequent observation of precipitation within the grains may be attributed to the relatively large initial austenite grain size. Similar features were observed in the case of V-bearing steel for V(C,N) particles. The experimental findings that niobium, even if in small amounts, was more efficient in strengthening and recrystallization retardation than vanadium was also confirmed by Kuziak et al. [26]. They reported that low niobium contents (<0.03%) give the best control over the strength properties in V–Nb steels also containing nitrogen [44]. In this work, it was found that the particle pinning-force hierarchy is: NbV(C,N) > Nb(C,N) > V(C,N) > AlN.

In the Nb-V-micro-alloyed steel, Nb and V both react with carbon and nitrogen to give carbides and nitrides, respectively. At 1,000 °C the solubility of vanadium is not at its maximum and thus V diffuses into the existing precipitate to give rise to the complex NbV(C,N) carbo-nitride. In the present study, as well as reported by Pandit et al. [22] for similar steels, no precipitates were found of the NbC, VC or VN type. All the vanadium is expected to remain in solid solution at the austenitizing temperature of 1,000 °C [56], whereas about 32% of the niobium precipitates as NbC and the rest of the niobium remains in solid solution. Atom probe analysis in [13] clearly showed that niobium was not forming Nb clusters or precipitates, but was randomly distributed as single atoms in the specimen held at 1,000 °C for 10 s after deformation [13].

Conclusions

Four micro-alloyed steels were microstructurally and mechanically investigated by using TEM and tensile tests to determine the effects of the Nb, V and Nb + V addition on the strain-induced ferrite transformation. The micro-strengthening mechanisms of the detected AlN, Nb(C,N), V(C,N) and NbV(C,N) carbo-nitrides, formed during the thermo-mechanical treatments, were determined using the Ashby-Orowan approach. Particles pinning force was calculated and compared to the recrystallization driving force. The main results can be summarized as follows:

- The calculated microstructure strengthening of the different precipitates (nitrides and carbo-nitrides), in all the four steels, showed a rather good correlation with the mechanical property data. The micro-strengthening contributions were found to average $0.8\sigma_y$.
- Addition of vanadium and niobium resulted in yield strength increase with respect to the vanadium or niobium containing steels.
- Particle pinning force was compared to the ferrite recrystallization driving force. This was rather small in the plain alloy containing little fraction of N and Al, whereas it was $\sim 0.15 \div 0.2$ in the two Nb and V steels, reaching its maximum ($\sim 0.30 \div 0.36$) in presence of NbV(C,N) particles, respect to the recrystallization driving force.

Acknowledgements The research has been partially funded by a MiUR–PRIN 2005 project. The authors wish to thank Ms. Silvia Saetti, Department of Engineering, University of Ferrara, and Mr. Alberto Fabrizi for their help in TEM specimen preparation.

References

1. Bakkaloglu A (2002) Mater Lett 56:200
2. Santos DB, Bruzszek RK, Rodrigues PCM, Pereloma EV (2003) Mater Sci Eng A 346:189. doi:10.1016/S0921-5093(02)00519-1
3. Kwon O, DeArdo AJ (1991) Acta Metall Mater 39:529. doi:10.1016/0956-7151(91)90121-G
4. Cruz MGH, Viecelli A (2008) Mater Des 29(2):539. doi:10.1016/j.matdes.2006.12.010
5. Yannacoppoulos S, Chaturvedi MC (1988) Can Metall Quart 27:163
6. Zajac S, Siwecki T, Hutchinson B (1991) Metall Mater Trans 22A:2681
7. Hodgson PD, Hickson MR, Gibbs RK (1999) Scr Mater 40:1179. doi:10.1016/S1359-6462(98)00411-4
8. Palmiere EJ, Garcia CI, DeArdo AJ (1994) Metall Mater Trans 25A:277
9. Pereloma EV, Timokhina IB, Russell KF, Miller MK (2006) Scr Mater 54:471. doi:10.1016/j.scriptamat.2005.10.008
10. Murayama M, Hono K (2001) Scr Mater 44:701. doi:10.1016/S1359-6462(00)00651-5
11. Hong SC, Lim SH, Hong HS, Lee KJ, Shin DH, Lee KS (2003) Mater Sci Eng A 355:241. doi:10.1016/S0921-5093(03)00071-6
12. Priestner R (1998) Mater Sci Forum 284–286:95
13. Maruyama M, Uemori R, Sugiyama M (1998) Mater Sci Eng A 250:2. doi:10.1016/S0921-5093(98)00528-0
14. Takaki S, Kawasaki K, Kimura Y (2001) J Mater Process Technol 117:359. doi:10.1016/S0924-0136(01)00797-X
15. Jonas JJ, Wiess I (1979) Meat Sci 13:238
16. Dutta B, Valdes A, Sellars CM (1992) Acta Metall Mater 40:653. doi:10.1016/0956-7151(92)90006-Z
17. LeBon A, Rofes-Vernis J, Rossard C (1975) Meat Sci 9:36
18. Rainforth WM, Black MP, Higginson RL, Palmiere EJ, Sellars CM, Prabst I et al (2002) Acta Mater 50:735. doi:10.1016/S1359-6454(01)00389-5
19. Craven AJ, He K, Garvie LAJ, Baker TN (2000) Acta Mater 48:3869. doi:10.1016/S1359-6454(00)00193-2
20. Stasko R, Adrian H, Adrian A (2006) Mater Charact 56:340. doi:10.1016/j.matchar.2005.09.012
21. Nes E, Ryum N, Hunderi O (1985) Acta Metall 33:11. doi:10.1016/0001-6160(85)90214-7
22. Pandit A, Murugaiyan A, Saha Podder A, Haldar A, Bhattacharjee D, Chandra S et al (2005) Scr Mater 53:1309. doi:10.1016/j.scriptamat.2005.07.003
23. Wilson JA, Craven AJ (2003) Ultramicroscopy 94:97. doi:10.1016/S0304-3991(02)00265-6
24. MacKenzie M, Craven AJ, Collins CL (2006) Scr Mater 54:1. doi:10.1016/j.scriptamat.2005.09.018
25. Hansen SS, Vander Sande JD, Cohen M (1980) Metall Trans 11A:387
26. Kuziak R, Bold T, Cheng Y-W (1995) J Mater Process Technol 53:255. doi:10.1016/0924-0136(95)01983-L
27. Gladman T (1997) The physical metallurgy of microalloyed steels. The Institute of Materials, London, pp 81–185, 263–355
28. Martin JW (1980) Micromechanisms in particle-hardened alloys. Cambridge solid state science series. Cambridge University Press, Cambridge, UK
29. Riva R, Mapelli C, Venturini R (2007) ISIJ Int 47:1204. doi:10.2355/isijinternational.47.1204
30. Cuddy LJ (1982) In: DeArdo AJ, Ratz GH, Wray PJ (eds) Thermomechanical processing of microalloyed austenite. TMS-AIME, Warrendale, PA, p 129
31. Azevedo G, Barbosa R, Pereloma EV, Santos D (2005) Mater Sci Eng A 402:98. doi:10.1016/j.msea.2005.04.026
32. Dutta B, Sellars CM (1987) Mater Sci Technol 3:197
33. Houghton DC (1993) Acta Metall Mater 41:2993. doi:10.1016/0956-7151(93)90114-8
34. Hong SG, Kang KB, Park CG (2002) Scr Mater 46:163. doi:10.1016/S1359-6462(01)01214-3
35. Chen G, Yang W, Guo S, Sun Z (2007) J Univ Sci Technol Beijing 14:36
36. Cao J-C, Liu Q-Y, Yong Q-L, Sun X-J (2007) J Iron Steel Res Int 14:51
37. Burke MG, Cuddy LJ, Piller J, Miller MK (1988) Mater Sci Technol 4:113
38. Kliber J, Schindler I (1996) J Mater Process Technol 60:597. doi:10.1016/0924-0136(96)02392-8
39. Cordea JN, Hook RE (1970) Metall Trans 1:111
40. Luton MJ, Dorvel R, Petkovic RA (1980) Metall Trans 11A:411
41. Rodrigues PCM, Pereloma EV, Santos DB (2000) Mater Sci Eng A 283:136. doi:10.1016/S0921-5093(99)00795-9
42. Singh AP, Prasad A, Prakash K, Sengupta D, Murty GMD (1999) Mater Sci Technol 15:121
43. Lee KJ, Lee JK (1999) Scr Mater 40:831. doi:10.1016/S1359-6462(99)00025-1
44. Maruyama N, Smith GDW (2002) Mater Sci Eng A327:34
45. DeArdo AJ (1998) Mater Sci Forum 284–286:15
46. Hong SG, Jun HJ, Kang KB, Park CG (2003) Scr Mater 48:1201. doi:10.1016/S1359-6462(02)00567-5
47. Mishra(Pathak) SK, Das S, Ranganathan S (2002) Mater Sci Eng A323:285. doi:10.1016/S0921-5093(01)01382-X
48. Pereloma EV, Timokhina IB, Miller MK, Hodgson PD (2007) Acta Mater 55:2587. doi:10.1016/j.actamat.2006.12.001
49. Hofer F, Warbichler P, Grogger W (1995) Ultramicroscopy 59:15. doi:10.1016/0304-3991(95)00015-S
50. Warbichler P, Hofer F, Hofer P, Letofsky E (1998) Micron 29:63. doi:10.1016/S0968-4328(97)00054-1
51. Petch NJ (1986) Acta Metall 34:1387. doi:10.1016/0001-6160(86)90026-X
52. Crooks MJ, Garratt-Reed AJ, Vander Sande JD, Owen WS (1981) Metall Trans 12A:1999
53. Pereloma EV, Boyd JD (1996) Mater Sci Technol 12:1043
54. Hulka K, Hillenbrand HG, Heisterkamp F, Niederhoff KA (1995) Microalloying 95. In: Proceedings of the international conference on microalloying, Pittsburg, PA, p 235
55. DeArdo AJ (1984) In: Dunne DP, Chandra T (eds) High strength low alloy steels. Wollongong University Press, NSW, p 70
56. Taylor KA (1995) Scr Metall 32:7. doi:10.1016/S0956-716X(99)80002-8
57. Garbarz B, Pickering FB (1988) Mater Sci Technol 4:967
58. Strid J, Easterling KE (1985) Acta Metall 33:2057. doi:10.1016/0001-6160(85)90129-4